

Last glacial maximum climate over China from PMIP simulations

Dabang Jiang^{a,b,c,*}, Xianmei Lang^d, Zhiping Tian^{a,e}, Donglin Guo^{a,e}

^a Nansen-Zhu International Research Centre, Institute of Atmospheric Physics, Chinese Academy of Sciences, Beijing, China

^b Key Laboratory of Regional Climate-Environment Research for Temperate East Asia, Chinese Academy of Sciences, Beijing, China

^c Climate Change Research Center, Chinese Academy of Sciences, Beijing, China

^d International Center for Climate and Environment Sciences, Institute of Atmospheric Physics, Chinese Academy of Sciences, Beijing, China

^e Graduate University of Chinese Academy of Sciences, Beijing, China

ARTICLE INFO

Article history:

Received 2 November 2010

Received in revised form 29 June 2011

Accepted 3 July 2011

Available online 13 July 2011

Keywords:

Last Glacial Maximum

Model-data comparison

Climate over China

ABSTRACT

Using the results of 25 climate models under the framework of the Paleoclimate Modelling Intercomparison Project (PMIP) and available proxy data, this study examines the regional climate of China during the Last Glacial Maximum (LGM: 21,000 years ago). Compared to the baseline climate, results show that annual surface temperature decreased by 2.00°–7.00 °C in China during that period, with an average of 4.46 °C, for the ensemble mean of all models. Annual precipitation and evaporation during the LGM were 5–40% less than the baseline values, with an average reduction of 20% (0.60 mm/day) and a reduction of 21% (0.41 mm/day) at the national scale, based on results from 15 out of the 25 models. These models were selected for their ability to simulate the modern precipitation climatology and for the availability of suitable evaporation data. Both the geographical distribution and magnitude of changes in surface temperature, precipitation, and evaporation during the LGM varied with the seasons and with the models, particularly at the sub-regional scale. Model-data comparisons revealed that the 25 models successfully reproduced the surface cooling trend during the LGM, but they failed to reproduce its magnitude in all four regions of comparison, particularly in the Hexi Corridor and in North and Northeast China. The simulations with computed sea surface temperatures (SSTs) were in better agreement with proxy estimates of surface temperature than those with prescribed SSTs. On the other hand, large-scale LGM-minus-baseline anomalies in annual precipitation minus evaporation agreed well, in a qualitative manner, with lake status-based reconstructions of changes in annual water budgets in East China and the region of 35°–42°N, 74°–97°E. On the eastern Qinghai–Tibetan Plateau, drier climates from the 15 models agreed with pollen-based reconstructions. For most parts of West China excluding the Qinghai–Tibetan Plateau, the simulations with computed (prescribed) SSTs are consistent (inconsistent) with reconstructed moister conditions.

© 2011 Elsevier B.V. All rights reserved.

1. Introduction

The Last Glacial Maximum (LGM) is well known as a cold period around 21,000 years before present. During that time, climate conditions were greatly different from those of today, with global surface temperature being reconstructed to be 4°–7 °C lower than the current level (Jansen et al., 2007). This provides a good opportunity for examining how the climate system responds to large changes in continental ice sheets and concentrations of atmospheric greenhouse gasses and dust content during glacial periods. In particular, the LGM has been a target period of the Paleoclimate Modelling Intercomparison Project (PMIP; Joussaume and Taylor, 1995; Braconnot et al., 2007).

Using atmospheric general circulation models (AGCMs) and regional climate models (RCM) nested within AGCMs, a few climate simulations have been conducted to address the East Asian and Chinese climates of the LGM (Wang and Zeng, 1993; Liu et al., 1995;

Chen et al., 2001; Yu et al., 2001; Liu et al., 2002; Jiang et al., 2003; Zhao et al., 2003; Zheng et al., 2004; Ju et al., 2007). They revealed that, with reference to the present day, annual surface temperatures decreased significantly over China, while annual precipitation decreased at the national scale during the LGM. On the other hand, model-model comparisons indicate a large spread in the magnitude of the LGM surface temperature changes and in the magnitude and sign of the LGM precipitation changes between the models. In most parts of western China, for example, wetter climates from an AGCM (Chen et al., 2001; Yu et al., 2001; Liu et al., 2002) starkly contrasted with drier climates from the rest of the models. These results were apparently model-dependent, implying a large degree of uncertainty in the LGM climate over China. Furthermore, this uncertainty became larger when the details of regional-scale and seasonal climate changes were taken into account. In this connection, it is of particular interest to integrate outputs from multiple climate models for analysis of the similarities and differences between the model results.

Ocean is an intrinsically interactive component of the climate system, and its effect has been regarded as an important mechanism contributing to the LGM climate (Jansen et al., 2007). However, the

* Corresponding author at: Nansen-Zhu International Research Centre, Institute of Atmospheric Physics, Chinese Academy of Sciences, Beijing, China.

E-mail address: jiangdb@mail.iap.ac.cn (D. Jiang).

earlier AGCM- and RCM-type simulations of the LGM climate over China were generally in line with the framework of the first phase of PMIP, and, therefore, had neglected ocean dynamics. Because these simulations underestimated the reconstructed changes in surface temperature over China as a whole (e.g., Jiang et al., 2003; Ju et al., 2007), what the LGM climate conditions over China were derived from coupled atmosphere–ocean general circulation models (AOGCMs), and then their degree of improved accuracy against proxy data over AGCMs remain to be resolved.

With the same or similar boundary conditions and experimental designs, a number of simulations of the LGM climate were performed using a hierarchy of climate models, ranging from AGCMs (either with prescribed SSTs or coupled with slab ocean models) to AOGCMs and coupled atmosphere–ocean–vegetation general circulation models (AOVGCMs), in the framework of PMIP (Joussaume and Taylor, 1995; Braconnot et al., 2007). These model results provide an excellent opportunity for investigating the common and different responses of climate models to the LGM forcings, model-dependent uncertainties, and the role of ocean on the regional climate over China.

On the other hand, using the PMIP simulations of the LGM climate, model-data comparisons have been carried out in the tropics (Pinot et al., 1999; Braconnot et al., 2007; Otto-Bliesner et al., 2009), the North Atlantic, Europe, and western Siberia (Kageyama et al., 2001, 2006; Ramstein et al., 2007), western Europe (Hoar et al., 2004), and Greenland and Antarctica (Masson-Delmotte et al., 2006). They have greatly advanced the understanding of climate change in those regions. In this area, however, we still have no knowledge about China. Based on a great deal of the reconstruction work, regional climate has been found to undergo dramatic changes in China during the LGM, particularly significantly lower surface temperatures than at present. These proxy data form a solid foundation upon which model-data comparisons can be made in a qualitative or quantitative manner. This begs the question as to the extent to which reconstructions and state-of-the-art simulations in China are compatible. Notably, unlike previous model-data comparisons based on individual AGCM results (e.g., Chen et al., 2001; Liu et al., 2002; Jiang et al., 2003; Yu et al., 2003; Ju et al., 2007), the comparisons between multiple climate models and a wealth of proxy data are more helpful for diagnosing the ability of current climate models to reproduce the East Asian monsoon climate during the LGM.

Importantly, insights gained from this regional scale study will contribute to a global perspective concerning model-data comparisons during the LGM.

Accordingly, an analysis was made of all the outputs available from the PMIP database to investigate the similarities and differences between the model results, the role of ocean on the regional climate, and the extent to which simulations are compatible with reconstructions over China during the LGM. The dynamical mechanisms behind the most common changes have also been discussed.

2. Data

2.1. Model, reanalysis, and proxy data

The present study examined all of the available simulations for the LGM climate under the framework of PMIP, including experiments using nine AGCMs with prescribed sea surface temperatures (SSTs) established by CLIMAP project members (1981) (SST-f) and eight AGCMs with SSTs computed by slab ocean models (SST-c) from the first phase of PMIP (PMIP1), plus six AOGCMs and one AOVGCM from the second phase of PMIP (PMIP2). The data of these 24 climate models were provided by the international modeling groups participating in PMIP and archived in the PMIP database from which we downloaded the data of interest. More information about the model data is available online at <http://pmip.lscce.ipsl.fr/>. In addition, a set of prescribed SST experiments performed using an AGCM developed at the Institute of Atmospheric Physics under the Chinese Academy of Sciences (Jiang et al., 2003; hereafter referred to as IAP) were also analyzed. Basic information about these 25 models is listed in Table 1.

Reanalysis data used to evaluate the ability of the models to reproduce the modern climatology over China included the National Centers for Environmental Prediction–National Center for Atmospheric Research (NCEP–NCAR) reanalysis of surface temperature (Kalnay et al., 1996) and the Climate Prediction Center (CPC) merged analysis of precipitation (Xie and Arkin, 1997) for the period 1979–2000. Given that there were differences of horizontal resolution among the models, all model and observation data of concern were aggregated to a relatively mid-range resolution of 96×48 (longitude \times latitude) using a linear interpolation or extrapolation approach.

Table 1
Basic information about the general circulation models used in the present study.

Model ID	Project	Atmospheric resolution (longitude \times latitude, level)	Length of run analyzed (year)	Baseline period	
01	BMRC2	PMIP1 (SST-f)	96 \times 80, L17	15	Modern
02	CCC2.0	PMIP1 (SST-f)	96 \times 48, L10	10	Modern
03	CCSR1	PMIP1 (SST-f)	64 \times 32, L20	10	Modern
04	ECHAM3	PMIP1 (SST-f)	128 \times 64, L19	10	Modern
05	GEN2	PMIP1 (SST-f)	96 \times 48, L18	10	Modern
06	IAP	PMIP1 (SST-f)	72 \times 46, L9	10	Modern
07	LMD4	PMIP1 (SST-f)	48 \times 36, L11	15	Modern
08	LMD5	PMIP1 (SST-f)	64 \times 50, L11	15	Modern
09	MRI2	PMIP1 (SST-f)	72 \times 46, L15	10	Modern
10	UGAMP	PMIP1 (SST-f)	128 \times 64, L19	20	Modern
11	CCC2.0-slab	PMIP1 (SST-c)	96 \times 48, L10	10	Pre-industrial
12	CCM1	PMIP1 (SST-c)	48 \times 40, L12	10	Pre-industrial
13	GEN1	PMIP1 (SST-c)	48 \times 40, L12	14	Pre-industrial
14	GEN2-slab	PMIP1 (SST-c)	96 \times 48, L18	10	Pre-industrial
15	GFDL	PMIP1 (SST-c)	96 \times 80, L20	25	Pre-industrial
16	MRI2-slab	PMIP1 (SST-c)	72 \times 46, L15	14	Pre-industrial
17	UGAMP-slab	PMIP1 (SST-c)	128 \times 64, L19	20	Pre-industrial
18	UKMO	PMIP1 (SST-c)	96 \times 73, L19	20	Pre-industrial
19	CNSM	PMIP2 (AOGCM)	128 \times 64, L18	100	Pre-industrial
20	CNRM	PMIP2 (AOGCM)	128 \times 64, L31	100	Pre-industrial
21	FGOALS	PMIP2 (AOGCM)	128 \times 60, L9	100	Pre-industrial
22	HadCM3M2	PMIP2 (AOGCM)	96 \times 73, L19	100	Pre-industrial
23	IPSL	PMIP2 (AOGCM)	96 \times 72, L19	100	Pre-industrial
24	MIROC3.2	PMIP2 (AOGCM)	128 \times 64, L20	100	Pre-industrial
25	HadCM3M2-veg	PMIP2 (AOVGCM)	96 \times 73, L19	100	Pre-industrial

To compare model results to proxy data, the reconstructions of the LGM surface temperature and moisture conditions were collected across China. The former was expressed in a quantitative manner, including records of pollen, ice core, sand wedge, stalagmite, organic fossil, phytolith, and halite from 130 sites. The latter was expressed in a qualitative manner, including lake records of 32 lakes and pollen data from nine sites. All of the proxy data and their corresponding references are represented in the model-data comparison section.

2.2. Boundary conditions for the LGM

The boundary conditions for modeling the LGM climate consisted of changes in the Earth's orbital parameters (Berger, 1978), ice-sheet extent, and the concentrations of atmospheric greenhouse gases. SSTs were prescribed as in CLIMAP project members (1981) for the PMIP1 SST-f experiments, but they were computed by slab ocean models in the PMIP1 SST-c experiments and by oceanic general circulation models in the PMIP2 experiments. The ICE-4G and ICE-5G ice-sheet reconstructions were respectively used in the PMIP1 and PMIP2 experiments (Peltier, 1994, 2004). Atmospheric CO₂ concentration varied from 345 ppm for the control run to 200 ppm for the LGM simulation in the PMIP1 experiments (Raynaud et al., 1993), while concentrations of atmospheric CO₂, CH₄, and N₂O varied from the pre-industrial values of 280 ppm, 760 ppb, and 270 ppb to 185 ppm, 350 ppb, and 200 ppb during the LGM in the PMIP2 experiments, respectively (Fluckiger et al., 1999; Dallenbach et al., 2000; Monnin et al., 2001). In addition, there were also differences in the baseline (or reference) period for the LGM climate simulations. The modern period ca. 1950 was used in the PMIP1 SST-f experiments, while the pre-industrial period ca. 1750 was used in the PMIP1 SST-c and PMIP2 experiments. More details about the boundary conditions and experimental designs of the LGM climate simulations can be found in Joussaume and Taylor (1995), Braconnot et al. (2007), and at the Web site <http://pmip.lscce.ipsl.fr/>.

2.3. Evaluation of the models

The extent to which climate models can reproduce the modern geographical distribution and magnitude of annual surface temperature and precipitation over China bears directly on whether their results are appropriate for addressing the LGM climate in this region. Therefore, spatial correlation coefficients (SCCs) and root-mean-square errors excluding systematic model error (RMSEs) of annual surface temperature and precipitation between each control simulation and observations were calculated on the basis of 77 grid points across the Chinese mainland. The former variable was used to quantify the similarity between simulated and observed spatial patterns, while the latter was used to assess internal model errors. With reference to the NCEP–NCAR reanalysis of surface temperature for the period 1979–2000 (Kalnay et al., 1996), Table 2 shows that SCCs ranged from 0.77 (CCSR1) to 0.99 (UKMO, HadCM3M2, and HadCM3M2-veg) and that RMSEs ranged from 1.19 °C (HadCM3M2) to 5.43 °C (CCSR1), indicating that the models were dependable in their ability to simulate the modern geographical distribution of annual surface temperature over China. Where the ensemble mean of the 25 models' results for annual surface temperature was concerned (equal weighting across models), the overall SCC and RMSE were 0.97 and 2.06 °C, respectively.

There was a large spread in the ability of the models to reproduce the modern annual precipitation over China, with reference to the CPC merged analysis of precipitation for the period 1979–2000 (Xie and Arkin, 1997). As listed in Table 2, SCCs ranged from –0.12 (GEN1) to 0.93 (HadCM3M2), and RMSEs ranged from 0.66 mm/day (HadCM3M2) to 3.47 mm/day (LMD4). To identify “reliable” models in terms of annual precipitation results, three criteria were arbitrarily set in this study. First, the SCC had to be positive and statistically significant at the 99% confidence level; second, the RMSE had to be <2 mm/day; and third, evaporation data had to be available, as precipitation minus

Table 2

Spatial correlation coefficients (SCC) and root-mean-square errors excluding systematic model error (RMSE) of annual surface temperature and precipitation between each baseline (or control) simulation and observations on the basis of 77 grid points within mainland China.

Model ID	Annual surface temperature		Annual precipitation		
	SCC	RMSE (°C)	SCC	RMSE (mm/day)	Analyzed or not
01 BMRC2	0.95	2.64	0.75	0.92	Yes
02 CCC2.0	0.88	3.95	0.52	1.51	Yes
03 CCSR1	0.77	5.43	0.79	0.81	Yes
04 ECHAM3	0.96	2.25	0.83	0.81	Yes
05 GEN2	0.95	2.52	0.82	1.06	Yes
06 IAP	0.89	3.60	0.69	1.16	No
07 LMD4	0.95	2.69	0.41	3.47	No
08 LMD5	0.97	2.52	0.66	2.24	No
09 MRI2	0.82	4.71	0.55	1.81	Yes
10 UGAMP	0.97	2.80	0.64	2.13	No
11 CCC2.0-slab	0.88	3.82	0.52	1.46	Yes
12 CCM1	0.78	5.22	0.79	1.09	Yes
13 GEN1	0.84	4.67	–0.12	1.41	No
14 GEN2-slab	0.95	2.56	0.84	1.17	Yes
15 GFDL	0.94	2.76	0.83	1.32	Yes
16 MRI2-slab	0.86	4.32	0.61	1.51	Yes
17 UGAMP-slab	0.97	2.67	0.64	2.17	No
18 UKMO	0.99	1.37	0.86	0.71	Yes
19 CCSM	0.94	2.80	0.69	0.96	No
20 CNRM	0.98	1.73	0.74	1.64	Yes
21 FGOALS	0.98	1.62	0.27	1.97	No
22 HadCM3M2	0.99	1.19	0.93	0.66	Yes
23 IPSL	0.96	2.51	0.60	1.08	No
24 MIROC3.2	0.95	2.75	0.79	0.86	No
25 HadCM3M2-veg	0.99	1.36	0.92	0.67	Yes

Observational climatology is derived from the NCEP–NCAR reanalysis of surface temperature (Kalnay et al., 1996) and the CPC merged analysis of precipitation (Xie and Arkin, 1997) for the period 1979–2000. For annual precipitation, SCCs with confidence levels <99% are in bold; RMSEs >2 mm/day are in bold; and models for which evaporation data is not available are listed in bold.

evaporation was used to evaluate net precipitation (or moisture) conditions during the LGM. In this manner, 15 models were finally chosen for analysis based on the results presented in Table 2. For the ensemble mean with equal weighting, the results of 15 models for annual precipitation in the baseline period gave a SCC of 0.87 and a RMSE of 0.74 mm/day. Taken together, the multi-model ensemble mean had a higher reliability with reference to most, but not all, of the individual models, which justifies our emphasis on the ensemble mean of the results of 25 models for annual surface temperature and the results of 15 models for precipitation in the following analyses.

3. LGM climate in China: results of PMIP simulations

3.1. Surface temperature

The LGM surface temperature differed greatly from that in the baseline period. In response to the LGM forcings, statistically significant annual surface temperature decreases of 2°–7 °C were obtained from the ensemble mean of the 25 models' experiments (hereafter referred to as MME-25) on the mainland of China (Fig. 1a). On the whole, surface temperature reductions intensified toward the high latitudes and were characterized by large changes in magnitude over most parts of the Qinghai–Tibetan Plateau and over Northeast China, where annual surface cooling exceeded 5 °C. For China as a whole, the MME-25 annual surface temperature decreased on average by 4.46 °C during the LGM with reference to the baseline climate. As seen in Table 3, although the LGM regionally averaged annual surface temperature in China was reduced consistently in the simulations of 25 models, the magnitude of the surface cooling was different among the models, ranging from 1.49 °C (BMRC2) to 9.32 °C (CCC2.0-slab), with a standard deviation of 1.68 °C across the models.

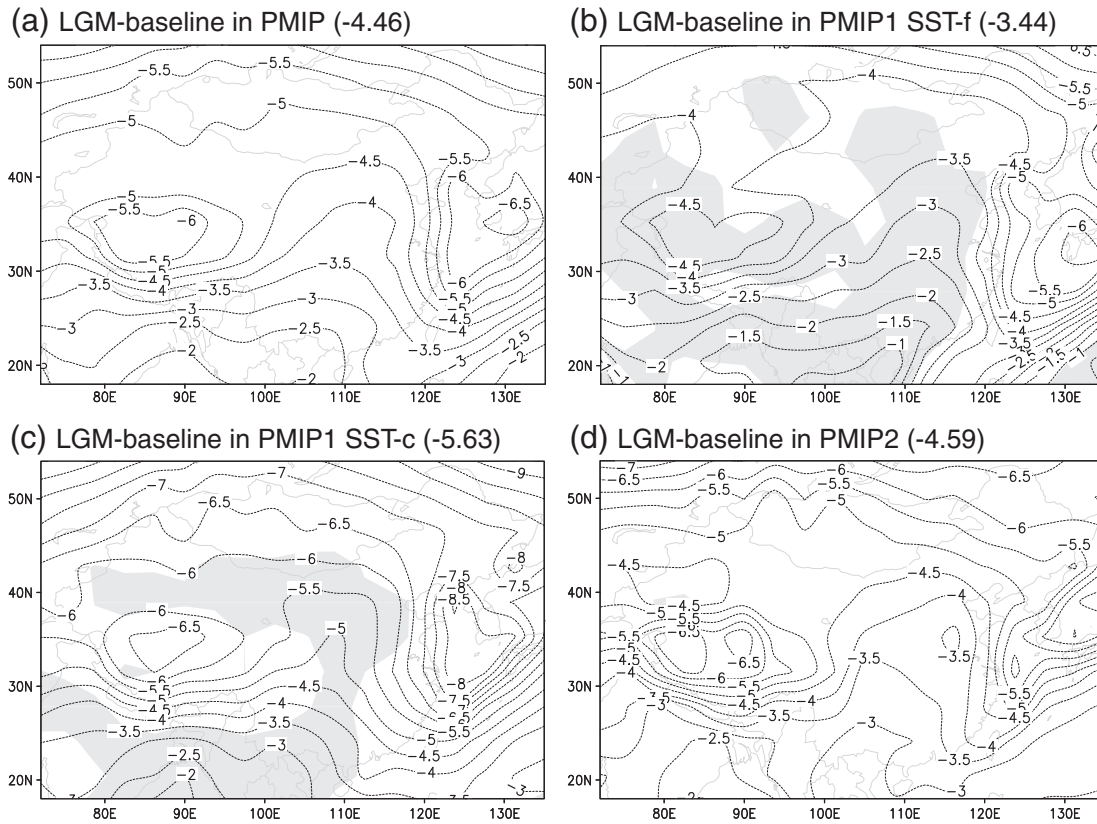


Fig. 1. LGM-baseline changes in annual surface temperature (units: °C) for (a) the ensemble mean of the 25 PMIP simulations, (b) the ensemble mean of the 10 PMIP1 SST-f simulations, (c) the ensemble mean of the eight PMIP1 SST-c simulations, and (d) the ensemble mean of the seven PMIP2 simulations. Areas with confidence levels <95% are shaded. Here, statistical significance is assessed by the use of a Student's *t*-test applied to the differences between the LGM and baseline simulations. Regionally averaged changes within the Chinese mainland are given in parentheses.

When viewed in terms of model classes, the geographical distribution of changes in the LGM annual surface temperature was similar across model types, but with different magnitudes (Fig. 1b–d). Annual surface cooling was the strongest in the ensemble mean of the eight PMIP1 SST-c experiments (-5.63 °C in China), whereas it was the weakest in the ensemble mean of the 10 PMIP1 SST-f experiments (-3.44 °C in China). Regionally averaged annual surface temperature in China was reduced by 4.59 °C in the ensemble mean of the seven PMIP2 experiments. Less surface cooling in the PMIP1 SST-f experiments with prescribed SSTs (CLIMAP project members, 1981) can be, at least partly, attributed to the small reductions in the reconstructed SSTs in the oceans adjacent to the East Asian continent. According to the availability of the SST data, the simulated changes in the LGM SSTs as derived from the six PMIP2 AOGCM simulations were compared to CLIMAP project members (1981). In the western North Pacific (0° – 40° N, 105° – 180° E) for example, the regionally averaged annual SST during the LGM was 2.34 °C (1.93 °C in FGOALS, 1.96 °C in CCSM, 2.03 °C in MIROC3.2, 2.49 °C in CNRM, 2.72 °C in IPSL, and 2.92 °C in HadCM3M2) colder than the baseline climate in the AOGCM experiments and was significantly stronger than the 1.24 °C SST decrease from CLIMAP project members (1981). Accordingly, the LGM annual surface cooling in China was larger in the AOGCM experiments, because the corresponding colder SSTs in the western North Pacific can give rise to larger losses of surface heat in the East Asian region during boreal warm seasons and smaller gains of surface heat during boreal cold seasons.

The geographical distribution of LGM-baseline anomalies in seasonal surface temperature varied with season and was generally similar to the annual mean pattern described above for East Asia, excluding ocean and near-ocean areas off the east coast of the Asian continent within the region of 30° – 40° N, 118° – 128° E. In this area, surface temperature changed by -10.0 °C to -14.0 °C in winter (December,

January, and February) and -3.0 °C to 1.0 °C in summer (June, July, and August), which was directly associated with the reconstructed land environment there rather than the modern ocean conditions, owing to a sea-level drop of ~ 120 m during the LGM relative to the present day (Peltier, 1994, 2004). For the whole of China, the LGM surface cooling differed in magnitude between the seasons, ranging from -3.85 °C in spring (March, April, and May) to -4.21 °C in summer to -4.60 °C in winter to -5.19 °C in autumn (September, October, and November) in terms of the MME-25 (Table 3). Moreover, the LGM change in surface temperature, with respect to the baseline climate, was largely different among the models in each season. It varied from 0.07 °C (BMRC2) to -9.37 °C (CCC2.0-slab) in spring, from -0.90 °C (IAP) to -10.26 °C (CCC2.0-slab) in summer, from -1.91 °C (BMRC2) to -10.71 °C (CCM1) in autumn, and from -1.55 °C (FGOALS) to -8.18 °C (CCC2.0-slab) in winter. Across the models, the smallest standard deviation was 1.64 °C in winter and the largest one was 1.99 °C in summer. In addition, as with the annual mean, in each season the magnitude of the surface temperature cooling was the strongest in the ensemble mean of the eight PMIP1 SST-c experiments, with values of -5.08 °C in spring, -5.29 °C in summer, -6.77 °C in autumn, and -5.39 °C in winter, whereas it was the weakest in the ensemble mean of the 10 PMIP1 SST-f experiments, with values of -2.78 °C in spring, -3.03 °C in summer, -3.92 °C in autumn, and -4.03 °C in winter. Surface temperature was reduced by 3.98 °C in spring, by 4.67 °C in summer, by 5.21 °C in autumn, and by 4.49 °C in winter for the ensemble mean of the seven PMIP2 experiments, respectively.

3.2. Precipitation

Annual precipitation was reduced by 5–40% in China during the LGM, with respect to the baseline climate, based on the ensemble

Table 3
LGM–baseline anomalies in regionally averaged annual surface temperature (units: °C) in China.

Model ID	Annual mean	Winter	Spring	Summer	Autumn
01 BMRC2	−1.49	−1.62	0.07	−2.49	−1.91
02 CCC2.0	−5.51	−3.69	−6.27	−6.65	−5.43
03 CCSR1	−3.26	−3.56	−3.03	−3.77	−2.69
04 ECHAM3	−2.77	−2.32	−1.24	−3.75	−3.78
05 GEN2	−3.96	−5.96	−2.56	−2.18	−5.13
06 IAP	−2.39	−3.94	−1.40	−0.90	−3.33
07 LMD4	−4.01	−5.92	−2.30	−2.37	−5.45
08 LMD5	−4.48	−5.95	−4.12	−3.06	−4.79
09 MRI2	−3.08	−3.47	−3.60	−1.86	−3.38
10 UGAMP	−3.47	−3.85	−3.38	−3.30	−3.35
11 CCC2.0-slab	−9.32	−8.18	−9.37	−10.26	−9.47
12 CCM1	−8.02	−7.70	−6.87	−6.78	−10.71
13 GEN1	−5.86	−5.74	−5.60	−5.15	−6.96
14 GEN2-slab	−3.48	−4.84	−2.41	−2.08	−4.59
15 GFDL	−4.25	−3.65	−3.45	−4.38	−5.50
16 MRI2-slab	−6.04	−5.01	−5.83	−6.06	−7.27
17 UGAMP-slab	−3.74	−3.51	−3.21	−3.78	−4.46
18 UKMO	−4.35	−4.54	−3.87	−3.82	−5.18
19 CCSM	−3.77	−3.97	−3.51	−3.55	−4.06
20 CNRM	−4.07	−5.19	−3.02	−3.40	−4.65
21 FGOALS	−3.65	−1.55	−3.61	−4.50	−4.93
22 HadCM3M2	−4.61	−4.90	−3.94	−4.55	−5.04
23 IPSL	−5.33	−4.66	−4.55	−5.93	−6.19
24 MIROC3.2	−4.07	−3.96	−3.38	−4.03	−4.92
25 HadCM3M2-veg	−6.61	−7.20	−5.82	−6.74	−6.67
MME-all	−4.46	−4.60	−3.85	−4.21	−5.19
MME-PMIP1-SST-f	−3.44	−4.03	−2.78	−3.03	−3.92
MME-PMIP1-SST-c	−5.63	−5.39	−5.08	−5.29	−6.77
MME-PMIP2	−4.59	−4.49	−3.98	−4.67	−5.21

MME-all denotes the ensemble mean of the 25 models; MME-PMIP1-SST-f denotes the ensemble mean of the 10 PMIP1 SST-f models; MME-PMIP1-SST-c denotes the ensemble mean of the eight PMIP1 SST-c models; and MME-PMIP2 denotes the ensemble mean of the seven PMIP2 models.

mean of the 15 models' experiments (hereafter referred to as MME-15) (Fig. 2a). Statistically significant changes in annual precipitation were registered in northern Northeast China, northernmost Xinjiang, the central part of the Qinghai–Tibetan Plateau, and Southeast China, where annual precipitation reductions were 20–40% of the baseline values. The spatial pattern and magnitude of the LGM changes in annual precipitation were similar overall between each of the three types of experiments, although there were differences, mostly in magnitude, at the sub-regional scale (Fig. 2b–d). Significantly, annual precipitation increased slightly in the PMIP1 SST-c experiments but decreased in the other two types of experiments in Southwest China. As listed in Table 4, at the national scale, regionally averaged annual precipitation was reduced by 20% (0.60 mm/day) in the MME-15 and was uniformly negative across the models, with a range of values from −6% (GFDL) to −38% (ECHAM3). On the whole, the LGM annual precipitation reduction was stronger in the ensemble mean of the six PMIP1 SST-f experiments (−27%) than that of the six PMIP1 SST-c experiments (−15%) or the three PMIP2 experiments (−17%).

The percentage change of seasonal precipitation during the LGM, relative to the baseline climate, was similar, both in sign and spatial pattern, between the seasons, and it agreed in general with the annual mean case over much of China. By contrast, there were also differences, both in sign and magnitude, in some parts of China. In the MME-15, for example, the LGM precipitation increased by 0–10% over most parts of Southwest China in winter and by 0–30% over the seas off the east coast of the East Asian continent around 35°N and 125°E in summer. However, it decreased by >40% in the latter region in both winter and autumn. On the other hand, regionally averaged precipitation in China uniformly decreased across the seasons in the MME-15, with values of −16% in spring, −21% in summer, −26% in autumn, and −14% in winter. Changes in the LGM seasonal precipitation were the same in sign but different in magnitude among the three types of experiments (Table 4).

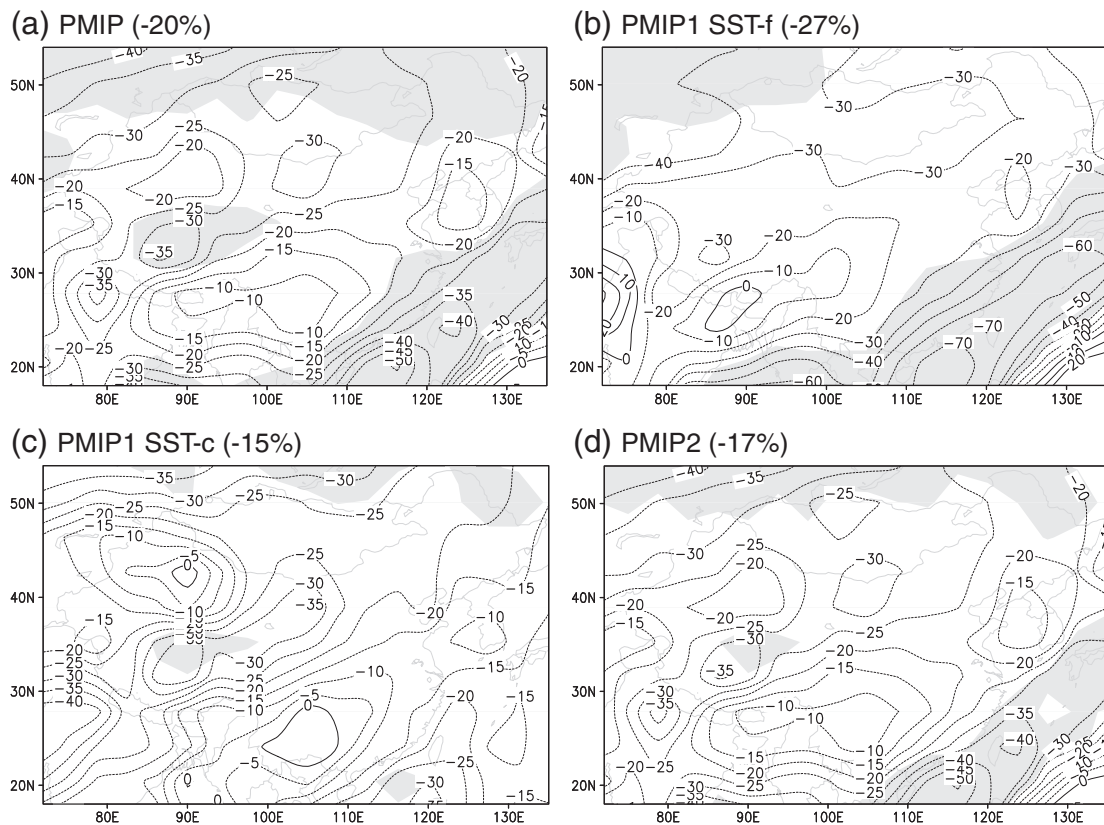


Fig. 2. Percentage changes in annual precipitation (units: %) during the LGM, with reference to the baseline climate, for (a) the ensemble mean of the 15 PMIP models, (b) the ensemble mean of the six PMIP1 SST-f models, (c) the ensemble mean of the six PMIP1 SST-c models, and (d) the ensemble mean of the three PMIP2 models. Areas with confidence levels >95% are shaded. Regionally averaged percentage changes within the Chinese mainland are given in parentheses.

Table 4
Percentage anomaly (units: %) and difference (units: mm/day, expressed in parentheses) of regionally averaged annual and seasonal precipitation and evaporation in China during the LGM with respect to the baseline climate.

Model ID	Precipitation/evaporation				
	Annual	Winter	Spring	Summer	Autumn
01 BMRC2	-25 (-0.67)/-29 (-0.51)	-49 (-0.45)/-56 (-0.37)	-25 (-0.72)/-25 (-0.50)	-10 (-0.47)/-18 (-0.49)	-47 (-1.03)/-43 (-0.67)
02 CCC2.0	-21 (-0.62)/-26 (-0.51)	8 (0.11)/-32 (-0.21)	-9 (-0.28)/-32 (-0.58)	-31 (-1.52)/-22 (-0.79)	-34 (-0.80)/-24 (-0.45)
03 CCSR1	-22 (-0.66)/-19 (-0.41)	1 (0.01)/-27 (-0.28)	-18 (-0.55)/-16 (-0.37)	-20 (-1.11)/-13 (-0.47)	-40 (-0.98)/-26 (-0.53)
04 ECHAM3	-38 (-0.77)/-34 (-0.49)	-43 (-0.27)/-53 (-0.37)	-34 (-0.65)/-34 (-0.48)	-24 (-0.90)/-18 (-0.41)	-71 (-1.25)/-50 (-0.71)
05 GEN2	-36 (-0.96)/-25 (-0.42)	-36 (-0.41)/-48 (-0.47)	-28 (-0.78)/-14 (-0.24)	-33 (-1.47)/-15 (-0.39)	-51 (-1.17)/-37 (-0.59)
09 MRI2	-24 (-1.05)/-18 (-0.53)	-26 (-0.48)/-19 (-0.25)	-18 (-0.92)/-16 (-0.50)	-29 (-1.99)/-18 (-0.83)	-22 (-0.81)/-21 (-0.54)
11 CCC2.0-slab	-17 (-0.48)/-32 (-0.64)	-3 (-0.05)/-48 (-0.34)	-22 (-0.67)/-46 (-0.87)	-20 (-1.00)/-26 (-0.92)	-9 (-0.20)/-22 (-0.42)
12 CCM1	-22 (-0.91)/-24 (-0.56)	-20 (-0.39)/-50 (-0.41)	-16 (-0.54)/-23 (-0.48)	-27 (-2.06)/-16 (-0.70)	-17 (-0.63)/-33 (-0.64)
14 GEN2-slab	-20 (-0.54)/-18 (-0.30)	-22 (-0.26)/-46 (-0.44)	-12 (-0.33)/-9 (-0.14)	-20 (-0.87)/-8 (-0.18)	-28 (-0.70)/-27 (-0.44)
15 GFDL	-6 (-0.20)/-9 (-0.16)	2 (0.03)/-22 (-0.16)	-3 (-0.13)/-8 (-0.19)	-6 (-0.32)/-3 (-0.10)	-16 (-0.39)/-14 (-0.21)
16 MRI2-slab	-13 (-0.49)/-16 (-0.41)	-8 (-0.13)/-25 (-0.32)	-13 (-0.55)/-17 (-0.45)	-17 (-0.98)/-11 (-0.42)	-8 (-0.29)/-19 (-0.46)
18 UKMO	-11 (-0.26)/-11 (-0.20)	-15 (-0.18)/-21 (-0.20)	-15 (-0.43)/-11 (-0.23)	-9 (-0.35)/-5 (-0.12)	-5 (-0.10)/-14 (-0.23)
20 CNRM	-13 (-0.41)/-17 (-0.25)	-7 (-0.07)/-34 (-0.24)	-7 (-0.20)/-12 (-0.18)	-15 (-0.88)/-9 (-0.22)	-21 (-0.51)/-25 (-0.38)
22 HadCM3M2	-16 (-0.41)/-19 (-0.33)	10 (0.09)/-37 (-0.31)	-12 (-0.35)/-14 (-0.26)	-21 (-1.02)/-13 (-0.35)	-18 (-0.35)/-26 (-0.41)
25 HadCM3M2-veg	-24 (-0.60)/-28 (-0.46)	-9 (-0.07)/-48 (-0.39)	-22 (-0.59)/-25 (-0.42)	-27 (-1.26)/-19 (-0.49)	-25 (-0.46)/-35 (-0.52)
MME-all	-20 (-0.60)/-21 (-0.41)	-14 (-0.17)/-36 (-0.32)	-16 (-0.51)/-20 (-0.39)	-21 (-1.08)/-15 (-0.46)	-26 (-0.65)/-27 (-0.48)
MME-PMIP1-SST-f	-27 (-0.79)/-24 (-0.48)	-21 (-0.25)/-37 (-0.32)	-21 (-0.65)/-21 (-0.44)	-25 (-1.24)/-18 (-0.56)	-41 (-1.01)/-31 (-0.58)
MME-PMIP1-SST-c	-15 (-0.48)/-19 (-0.38)	-11 (-0.16)/-35 (-0.31)	-13 (-0.44)/-19 (-0.39)	-17 (-0.93)/-12 (-0.41)	-14 (-0.39)/-22 (-0.40)
MME-PMIP2	-17 (-0.47)/-21 (-0.35)	-2 (-0.02)/-40 (-0.31)	-13 (-0.38)/-17 (-0.29)	-21 (-1.05)/-14 (-0.35)	-21 (-0.44)/-29 (-0.44)

MME-all denotes the ensemble mean of the 15 models; MME-PMIP1-SST-f denotes the ensemble mean of the six PMIP1 SST-f models; MME-PMIP1-SST-c denotes the ensemble mean of the six PMIP1 SST-c models; and MME-PMIP2 denotes the ensemble mean of the three PMIP2 models.

The percentage anomalies of regionally averaged seasonal precipitation were obviously stronger in the six PMIP1 SST-f simulations than in the nine PMIP1 SST-c and PMIP2 simulations. In addition, in each season, the LGM changes in regionally averaged seasonal precipitation were greatly different between the models, with a wide range of values from -3% (GFDL) to -34% (ECHAM3) in spring, from -6% (GFDL) to -33% (GEN2) in summer, from -5% (UKMO) to -71% (ECHAM3) in autumn, and from 10% (HadCM3M2) to -49% (BMRC2) in winter.

3.3. Evaporation

During the LGM, annual evaporation in China was reduced by 5–40% in the MME-15, which was related directly to the LGM surface cooling. Statistically significant reductions in annual evaporation occurred mainly in East China and for the central and western Qinghai-Tibetan Plateau, with negative anomalies of 15% to 40% (Fig. 3a). The magnitude of change in annual evaporation during the

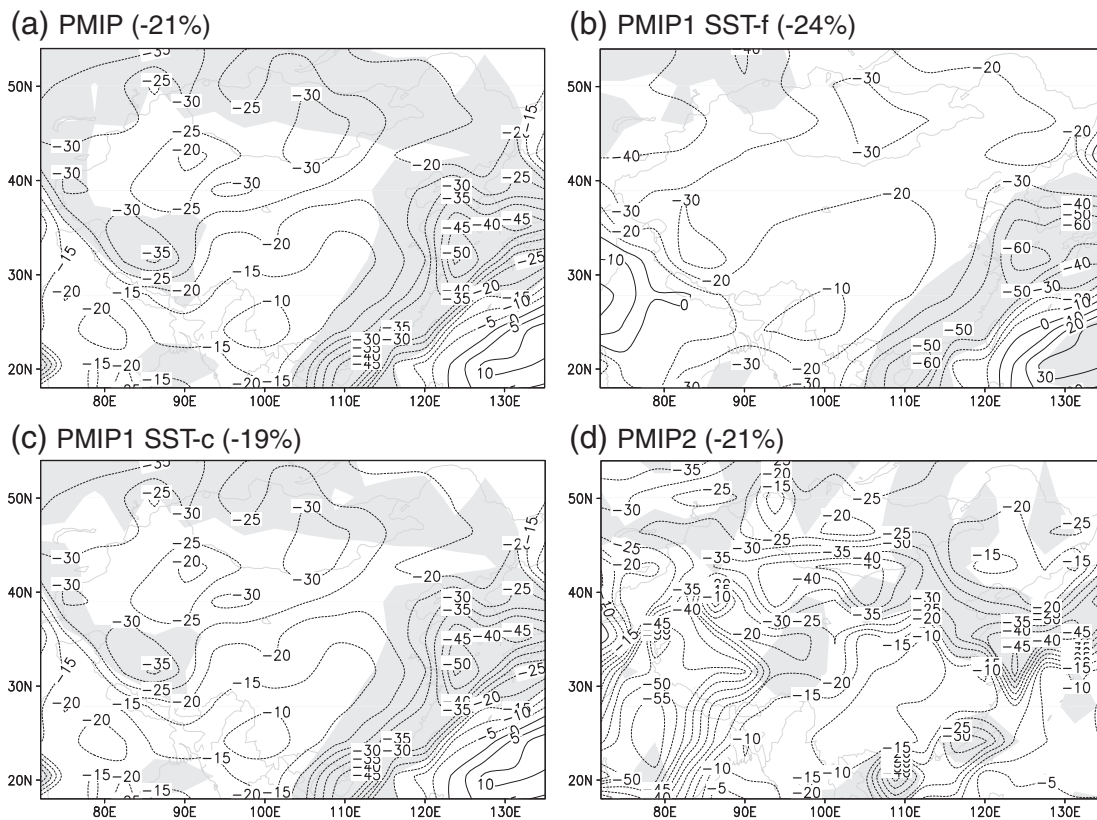


Fig. 3. Same as Fig. 2, but for percentage changes in annual evaporation (units: %).

Table 5Proxy data providing estimates of changes (LGM–present) in annual surface temperature (ΔT_{ann} ; units: °C) over the Chinese mainland.

Site	Proxy data	Region	ΔT_{ann}	Reference
12 sites in South China	Pollen	20°–32°N, 105°–120°E	-7 ± 3.5	Farrera et al. (1999) and references therein
Tianyang Lake borehole	Pollen	20.31°N, 110.18°E	–5 to –8	Zheng and Guiot (1999)
Seven sites in the Qinghai-Tibetan Plateau	Ice core, pollen, and sand wedge	28°–36°N, 80°–100°E	–6 to –9, with an average of –7	Shi et al. (1997), Shi (2002), and references therein
Seven sites in the eastern Qinghai-Tibetan Plateau	Pollen	30°–37°N, 92°–102°E	–6	Tang et al. (1998)
Hulu Cave	Stalagmite	32.30°N, 119.10°E	Around –8	Wang et al. (2002)
80 sites in North and Northeast China	Pollen	34°–50°N, 105°–135°E	At least –8 to –10	Liu (1988)
Weinan loess-paleosol sequence	Organic fossil	34.24°N, 109.30°E	–7 to –9	Wu et al. (1994)
Weinan loess-paleosol sequence	Phytolith	34.24°N, 109.30°E	–6.2 to –6.6	Lu et al. (2007)
Guliya ice cap	Ice core	35.17°N, 81.29°E	colder than –9	Yao et al. (2000)
Two boreholes in the Chaerhan Salt Lake	Halite	36.37°–37.12°N, 94.15°–96.14°E	–6 to –7	Zhang et al. (1995)
Luanhaizi Lake	Pollen	37.59°N, 101.35°E	–4 to –7	Herzschuh et al. (2006)
11 sand deposit sites in northwestern Shanxi Province	Pollen	38°–41°N, 111°–113°E	–9.6 to –15.5	Su and Ma (1997)
Six sites in the Hexi Corridor	Sand wedge	39°–41°N, 94°–100°E	–13 to –15	Wang et al. (2001)

LGM was similar, but its spatial pattern was somewhat different between each of the three types of experiments (Fig. 3b–d). For example, large reductions of >30% obtained for annual evaporation in the PMIP1 SST-f and SST-c experiments were not observed in the three PMIP2 experiments in Southeast China. The spatial variability of the LGM annual evaporation change was larger in the PMIP2 experiments than in the remaining experiments, particularly in West China and North China, which was probably connected to the smaller number of climate models in the PMIP2 experiments. Table 4 indicates that the LGM regionally averaged annual evaporation in China decreased in all the PMIP experiments, ranging from –9% (GFDL) to –34% (ECHAM3), and it was reduced by an average of 21% (0.41 mm/day) in the MME-15. Moreover, the magnitude of the LGM change in regionally averaged annual evaporation was comparable between each of the three types of experiments, with values of –24% in the PMIP1 SST-f simulations, –19% in the PMIP1 SST-c simulations, and –21% in the PMIP2 simulations.

Seasonal evaporation during the LGM was reduced overall in China, with a magnitude similar to the annual mean results on a large scale. At the sub-regional scale, however, the percentage change in the LGM seasonal evaporation differed by season, particularly over and around the region of 30°–40°N, 118°–128°E. In this area, the LGM evaporation was reduced by >40% in winter and autumn but was increased by >40% in summer, which was related directly to the LGM surface temperature anomalies described previously and can be attributed to the assigned changes in surface boundary condition from the modern ocean conditions to the reconstructed land conditions during the LGM (Peltier, 1994, 2004). As shown in Table 4, the LGM regionally averaged seasonal evaporation in China was reduced by 20% in spring, 15% in summer, 27% in autumn, and 36% in winter on the basis of the MME-15. This change

was uniformly negative across the 15 models, with a wide range of values from –8% (GFDL) to –46% (CCC2.0-slab) in spring, from –3% (GFDL) to –26% (CCC2.0-slab) in summer, from –14% (GFDL and UKMO) to –50% (ECHAM3) in autumn, and from –19% (MRI2) to –56% (BMRC2) in winter. Moreover, in each season, the percentage change in the LGM evaporation was comparable in magnitude between each of the three types of experiments and was near the average value as derived from the MME-15.

4. Model-data comparison

4.1. Surface temperature

Quantitative reconstructions of the LGM surface temperature changes as derived from a variety of proxy records at 130 sites, together with the related information, have been summarized in Table 5. Because the density of geographical distribution of the reconstructions was very uneven, four regions covering most parts of China were selected in terms of the spatial coverage of the proxy data for performing model-data comparisons in a regional context. In each region, reconstructed surface temperatures were first obtained through a collection of all results of the proxy data on sites inside, and then they were compared to regionally averaged annual surface temperature changes of all values of the grid points inside from the models. According to the results listed in Table 6, proxy estimates of annual surface temperatures during the LGM were uniformly negative compared to the present-day values, with differences of -7.0 ± 3.5 °C in South China, –6 °C to –9 °C over the Qinghai–Tibetan Plateau, –13 °C to –15 °C in the Hexi Corridor, and at least –8 °C to –10 °C in North and Northeast China. In the MME-25, regionally averaged annual surface temperature during the LGM was

Table 6Model-data comparison of ΔT_{ann} (units: °C) in four regions of China.

Reconstructions and experiments	ΔT_{ann} in each region			
	South China	Qinghai-Tibetan Plateau	Hexi Corridor	North and Northeast China
Reconstructions	-7.0 ± 3.5	–6 to –9	–13 to –15	At least –8 to –10
MME-all	–3.39 (1.77)	–5.05 (2.46)	–4.68 (1.47)	–4.86 (1.92)
MME-PMIP1-SST-f	–2.23 (1.30)	–4.07 (1.39)	–3.89 (1.16)	–3.67 (1.50)
MME-PMIP1-SST-c	–4.77 (1.89)	–5.81 (3.47)	–5.68 (1.57)	–6.40 (1.84)
MME-PMIP2	–3.48 (0.89)	–5.56 (1.68)	–4.65 (0.99)	–4.82 (1.14)
HadCM3M2	–3.46	–5.94	–4.66	–4.58
HadCM3M2-veg	–4.71	–8.99	–5.77	–7.10

MME-all denotes the ensemble mean of the 25 models; MME-PMIP1-SST-f denotes the ensemble mean of the 10 PMIP1 SST-f models; MME-PMIP1-SST-c denotes the ensemble mean of the eight PMIP1 SST-c models; and MME-PMIP2 denotes the ensemble mean of the seven PMIP2 models. The regions are defined as follows: South China (20°–33°N, 105°–120°E), Qinghai–Tibetan Plateau (28°–37°N, 80°–102°E), Hexi Corridor (39°–41°N, 94°–100°E), and North and Northeast China (34°–50°N, 105°–135°E). Oceanic regions and land regions not belonging to China are excluded when regionally averaged values are calculated in each region. The standard deviation (units: °C) of model results is in italics inside parentheses.

reduced by 3.39 °C in South China, by 5.05 °C over the Qinghai–Tibetan Plateau, by 4.68 °C in the Hexi Corridor, and by 4.86 °C in North and Northeast China, respectively. All of these results were smaller than the reconstructed levels. In other words, the PMIP models successfully reproduced the surface cooling trend during the LGM but failed to reproduce its magnitude in these areas, particularly in the latter two regions. When inter-model variability of simulated surface temperature changes, represented by the standard deviation of model results about their mean, was taken into account, the MME-25 lay in the low range of proxy estimates for South China and the Qinghai–Tibetan Plateau regions. However, the model–data discrepancies were still substantial in magnitude and still could not be reconciled in the remaining two regions.

As with the case of the whole of China, the magnitude of annual surface temperature changes during the LGM differed between the model classes, with the largest being for the 10 PMIP1 SST-c experiments and the smallest being for the eight PMIP1 SST-f experiments in all the four regions (Table 6). The results of the seven PMIP2 experiments lay in the range between the PMIP1 SST-c and SST-f experiments. Meanwhile, the model spread was also the largest in the PMIP1 SST-c experiments in the four regions where the standard deviation of the model results varies from 1.57 °C to 3.47 °C (depending on the region). In general, the PMIP1 SST-c experiments were in the best agreement and the SST-f experiments were in the poorest agreement with proxy estimates of surface temperature among the PMIP experiments, and the PMIP experiments with computed SSTs were in better agreement with proxy estimates than those with prescribed SSTs. This means that an interactive ocean played an important role in forming climate conditions of China during the LGM.

4.2. Precipitation minus evaporation

Unlike most previous studies comparing simulated precipitation changes directly to the dry/wet conditions estimated by proxy data (e.g., Pinot et al., 1999; Kageyama et al., 2001; Jiang et al., 2003; Hoar et al., 2004; Braconnot et al., 2007), simulated LGM–baseline (or LGM–

minus-baseline) anomalies in precipitation minus evaporation (P–E, an appropriate variable to represent moisture conditions) were first analyzed and then compared to reconstructions in this subsection. In terms of the MME-15, annual P–E decreased by 0.00–0.60 mm/day in China excluding parts of western China (around 35°–42°N, 74°–97°E) and southeastern Sichuan Province (near 28°N, 105°E) where annual P–E increased by <0.10 mm/day (Fig. 4a). At the national scale, regionally averaged annual P–E during the LGM was decreased by 18% (0.19 mm/day) in China relative to a baseline annual P–E value of 1.07 mm/day. LGM–baseline anomalies in annual P–E differed among the models, particularly with a positive value (0.16 mm/day) obtained by CCC2.0-slab, and between each of the three types of experiments, with values of –33% (–0.31 mm/day) from the six PMIP1 SST-f models, –9% (–0.10 mm/day) from the six PMIP1 SST-c models, and –12% (–0.13 mm/day) from the three PMIP2 models. In addition, seasonal mean P–E during the LGM increased by 39% (0.15 mm/day) in winter but decreased by 10% (0.12 mm/day) in spring, by 30% (0.62 mm/day) in summer, and by 24% (0.16 mm/day) in autumn. As such, annual P–E reductions during the LGM mainly resulted from larger reductions in the seasonal mean P–E in summer, which was due to a larger decrease in precipitation (1.08 mm/day) than evaporation (0.46 mm/day). Notably, in response to changes in zonal and meridional surface temperature gradients across the Asian-Pacific areas, all 14 PMIP models for analysis reproduced a weaker than baseline summer monsoon over East Asia, with an average decrease of 25%, during the LGM (Jiang and Lang, 2010). Such a systematic weakening of the monsoon circulation was most responsible for the aforementioned precipitation decrease over China during the LGM summer, as summer precipitation in this region is dominated by monsoon (Tao and Chen, 1987).

According to records of lake level, water depth, lake area, and water salinity of 32 lakes, Yu et al. (2003) compiled a set of lake status data on qualitative changes of the annual water budget during the LGM. Combined with other lines of evidence, they revealed that the LGM climate was drier in eastern China but somewhat wetter in western China than at present. On a large scale, LGM–baseline

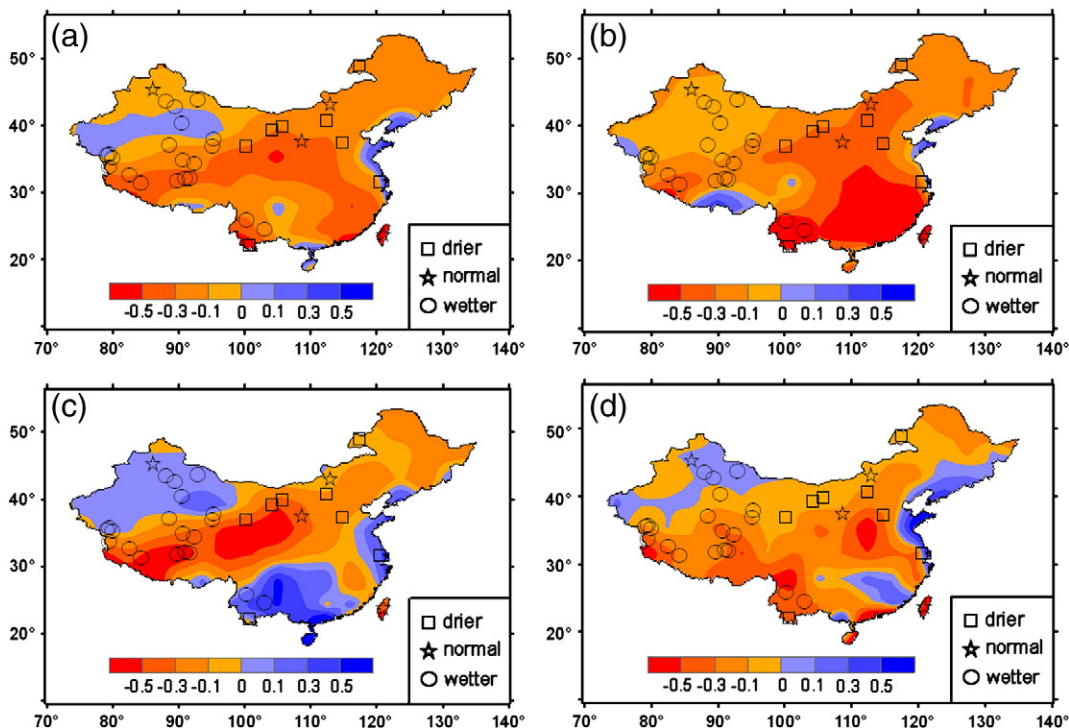


Fig. 4. LGM–baseline changes in annual P–E (shading, units: mm/day) for (a) the ensemble mean of the 15 PMIP models, (b) the ensemble mean of the six PMIP1 SST-f models, (c) the ensemble mean of the six PMIP1 SST-c models, and (d) the ensemble mean of the three PMIP2 models. Also shown is the lake status-based reconstruction of changes in water balance during the LGM (Yu et al., 2003), in which open squares represent drier conditions, open circles represent wetter conditions, and open stars represent normal conditions.

anomalies in annual P–E from the MME-15 agreed well with these lake status-based reconstructions of moisture conditions over most parts of China (Fig. 4a). Among these anomalies were drier conditions in East China east of $\sim 100^\circ\text{E}$ and wetter conditions in the region defined roughly by $35^\circ\text{--}42^\circ\text{N}$, $74^\circ\text{--}97^\circ\text{E}$. By contrast, model-data disagreements occurred over the Qinghai–Tibetan Plateau and most parts of northern Xinjiang, where simulated drier conditions were opposite the wetter conditions estimated by reconstructed higher lake levels and fresher water than the modern period during the LGM (Yu et al., 2003). However, it is worth noting that, contrary to the wetter conditions derived from lake status records, the pollen data from nine sampling sites covering the eastern Qinghai–Tibetan Plateau ($29^\circ\text{--}37^\circ\text{N}$, $92^\circ\text{--}102^\circ\text{E}$) suggested a much drier climate during the LGM (Tang et al., 1998, 2004; Wan et al., 2008). Because lake status on the Qinghai–Tibetan Plateau was significantly affected by melt water of mountain glaciers, with probably more water supply during the glacial times, pollen-based reconstructions were certainly better than the lake status data, although the effects of melt water also persisted, but in a minor degree. In this connection, drier climate of the MME-15 qualitatively agreed with proxy data on the eastern Qinghai–Tibetan Plateau. Moreover, the LGM annual precipitation was reduced by 15–40% on the Qinghai–Tibetan Plateau in terms of the MME-15 (Fig. 2a), which was also compatible with the 30–70% reduction in annual precipitation deduced by Shi et al. (1997).

Fig. 4b–d shows that, although there are differences both in the spatial pattern and magnitude of changes in annual P–E during the LGM between each of the three types of PMIP experiments, drier-than-baseline conditions occurred overall in East China east of $\sim 100^\circ\text{E}$ and over the Qinghai–Tibetan Plateau across these experiments. Apparent disagreements between the model classes appeared in West China excluding the Qinghai–Tibetan Plateau: regionally drier conditions were obtained by the six PMIP1 SST-f models and opposite results were derived from the six PMIP1 SST-c models and three PMIP2 models. In this regard, the PMIP simulations with computed (prescribed) SSTs were consistent (inconsistent) with proxy data in these regions during the LGM. Additionally, for the Qinghai–Tibetan Plateau, annual P–E remained constant or increased by ~ 0.50 mm/day in an AGCM experiment, which was then used to explain wetter conditions during the LGM (Chen et al., 2001; Yu et al., 2001). Based on the present study, this cause-and-effect relationship is obviously model-dependent, as the annual P–E during the LGM was reduced uniformly in the ensemble mean of the PMIP simulations with either prescribed or computed SSTs (Fig. 4).

5. Conclusion

In this study, the LGM climate over China was investigated using the PMIP simulations from 10 AGCMs with prescribed SSTs, eight AGCMs coupled with slab ocean models, six AOGCMs, and one AOVGCM. The primary conclusions are as follows:

- (1) All 25 models reproduced a colder-than-baseline climate in China during the LGM, and the regionally averaged annual surface temperature was reduced by 4.46°C , ranging from 1.49°C to 9.32°C depending on the model. Surface cooling was greater in the simulations with computed SSTs than those with prescribed SSTs, and the smaller magnitude in the latter can be, at least partly, attributed to a systematic weakness of reconstructed changes in SSTs (CLIMAP project members, 1981) in the oceans adjacent to East Asia.
- (2) During that period, both annual precipitation and evaporation in China were reduced across the simulations from all the 15 models chosen for analysis. Larger reductions in precipitation rather than evaporation gave rise to a drier-than-baseline climate over much of China during the LGM. At the national

scale, the LGM annual P–E was reduced by 18% (0.19 mm/day) compared to the baseline climate.

- (3) The 25 models, in general, underestimated the magnitude of surface cooling during the LGM, as suggested by proxy data, for all the four regions of China where model-data comparison was performed. The simulations with computed SSTs were in better agreement with proxy estimates of surface temperature than those with prescribed SSTs. On the other hand, the 15-model simulated large-scale LGM–baseline anomalies in annual P–E qualitatively agreed with lake status-based reconstructions of changes in annual water budgets over China excluding the Qinghai–Tibetan Plateau and northern Xinjiang. On the eastern Qinghai–Tibetan Plateau, drier climates from the 15 models agreed (disagreed) with pollen (lake status) data.

Taken together, the first lesson learned from the present study is that the ocean was an important component of the climate system in the East Asian monsoon area during the LGM: the simulations with interactive oceans were in better agreement with proxy estimates than the PMIP1 SST-f simulations in China. In this connection, the response of the ocean to the LGM forcings needs to be accounted for using the PMIP2 simulations to understand the role of ocean feedback on the East Asian climate during the LGM. In addition, simulated annual surface temperature during the LGM was lower in the PMIP1 SST-c simulations than in the PMIP2 simulations for all the regions of model-data comparison, with an additional cooling of 1.29°C in South China, 0.25°C for the Qinghai–Tibetan Plateau, 1.03°C in the Hexi Corridor, and 1.58°C in North and Northeast China (Table 6). This raises the question: Why do AGCMs coupled with simple slab ocean models tend to do a better job with reference to comparisons to proxy evidence? It is a pity that SSTs from the PMIP1 SST-c simulations were not available in the PMIP database, making it impossible to perform further investigation in this respect.

Vegetation feedback has been proposed as an important process contributing to the LGM climate (e.g., Crowley and Baum, 1997; Levis et al., 1999; Crucifix and Hewitt, 2005; Jansen et al., 2007; Jiang, 2008). Using AGCMs with reconstructed vegetations, earlier simulations of the LGM climate showed that changes in vegetation induced additional climate change, which in general reduced model-data disagreements in surface temperature over China (Chen et al., 2001; Yu et al., 2001; Jiang et al., 2003). The PMIP2 simulations using HadCM3M2 and HadCM3M2-veg provide an opportunity to evaluate the effect of vegetation on the East Asian climate in a fully coupled climate model context during the LGM, as the dynamical vegetation model is the main difference between the two models (Michel Crucifix, personal communication, 2009). Averaged across the whole country, annual surface temperature during the LGM was 2.00°C colder in HadCM3M2-veg (-6.61°C) than in its AOGCM counterpart (-4.61°C), and seasonal surface temperature was also much colder in the former than it was in the latter (Table 3). At the regional scale, it was further reduced by 1.25°C in South China, by 3.05°C over the Qinghai–Tibetan Plateau, by 1.11°C in the Hexi Corridor, and by 2.52°C in North and Northeast China in HadCM3M2-veg compared to HadCM3M2 (Table 6). Accordingly, the results of surface temperature obtained in HadCM3M2-veg were more consistent with proxy estimates in China, particularly in South China and for the Qinghai–Tibetan Plateau where this simulation agreed well with proxy records (Table 6). In this analysis, the vegetation appeared to be another important component in determining the East Asian climate during the LGM, although the underlying mechanism needs to be further explored.

In addition to the models themselves, another possible source that may be at least partly responsible for the model-data mismatch is the uncertainty in the proxy data. This is especially true for the eastern Qinghai–Tibetan Plateau, where wetter conditions derived from lake status records (Yu et al., 2003) were opposite of the drier conditions derived from pollen records during the LGM (Tang et al., 1998, 2004; Wan et al., 2008). Given that the spatial coverage of the proxy data used for the present model-data comparison was rather sparse, more

reconstruction work using a variety of proxy data and methods is urgently needed to test model results and, hence, to improve our knowledge of the LGM climate in the East Asian monsoon area.

Acknowledgements

We sincerely thank the two anonymous reviewers for their helpful comments and suggestions on the manuscript. Also, we acknowledge the international modeling groups for providing their data for analysis, and the Laboratoire des Sciences du Climat et de l'Environnement (LSCE) for collecting and archiving the model data. This research was supported by the Chinese National Basic Research Program (2009CB421407), the Strategic Priority Research Program (XDA05120703) and the Knowledge Innovation Program (KZCX2-EW-QN202) of the Chinese Academy of Sciences, and by the National Natural Science Foundation of China (40775052 and 40975050). The PMIP2/MOTIF Data Archive is supported by CEA, CNRS, the EU project MOTIF (EVK2-CT-2002-00153) and the Programme National d'Etude de la Dynamique du Climat (PNEDC). The analyses were performed using version 27 December 2008 of the database. More information is available on <http://pmip2.lsce.ipsl.fr/> and <http://motif.lsce.ipsl.fr/>.

References

- Berger, A.L., 1978. Long-term variations of daily insolation and Quaternary climatic changes. *Journal of the Atmospheric Sciences* 35, 2362–2367.
- Braconnot, P., Otto-Bliesner, B., Harrison, S., Joussaume, S., Peterchmitt, J.-Y., Abe-Ouchi, A., Crucifix, M., Driesschaert, E., Fichet, Th., Hewitt, C.D., Kageyama, M., Kitoh, A., Laine, A., Loutre, M.-F., Marti, O., Merkel, U., Ramstein, G., Valdes, P., Weber, S.L., Yu, Y., Zhao, Y., 2007. Results of PMIP2 coupled simulations of the Mid-Holocene and Last Glacial Maximum – part 1: experiments and large-scale features. *Climate of the Past* 3, 261–277.
- Chen, X., Yu, G., Liu, J., 2001. An AGCM + SsIB model simulation on changes in palaeomonsoon climate at 21 ka BP in China. *Acta Meteorologica Sinica* 15, 333–345.
- CLIMAP project members, 1981. Seasonal reconstructions of the Earth's surface at the Last Glacial Maximum. Geological Society of America Map Chart Series MC-36. Geol. Soc. Am. Boulder, Colorado.
- Crowley, T.J., Baum, S.K., 1997. Effect of vegetation on an ice-age climate model simulation. *Journal of Geophysical Research* 102 (D14), 16463–16480.
- Crucifix, M., Hewitt, C.D., 2005. Impact of vegetation changes on the dynamics of the atmosphere at the Last Glacial Maximum. *Climate Dynamics* 25, 447–459.
- Dallenbach, A., Blunier, T., Fluckiger, J., Stauffer, B., Chappellaz, J., Raynaud, D., 2000. Changes in the atmospheric CH₄ gradient between Greenland and Antarctica during the Last Glacial and the transition to the Holocene. *Geophysical Research Letters* 27, 1005–1008.
- Farrera, I., Harrison, S.P., Prentice, I.C., Ramstein, G., Guiot, J., Bartlein, P.J., Bonnefille, R., Bush, M., Cramer, W., von Grafenstein, U., Holmgren, K., Hooghiemstra, H., Hope, G., Jolly, D., Lauritzen, S.-E., Ono, Y., Pinot, S., Stute, M., Yu, G., 1999. Tropical climates at the Last Glacial Maximum: a new synthesis of terrestrial palaeoclimate data. I. Vegetation, lake-levels and geochemistry. *Climate Dynamics* 15, 823–856.
- Fluckiger, J., Dallenbach, A., Blunier, T., Stauffer, B., Stocker, T.F., Raynaud, D., Barnola, J.M., 1999. Variations in atmospheric N₂O concentration during abrupt climatic changes. *Science* 285, 227–230.
- Herzschuh, U., Kürschner, H., Mischke, S., 2006. Temperature variability and vertical vegetation belt shifts during the last ~50,000 yr in the Qilian Mountains (NE margin of the Tibetan Plateau, China). *Quaternary Research* 66, 133–146.
- Hoar, M.R., Palutikof, J.P., Thorne, M.C., 2004. Model intercomparison for the present day, the mid-Holocene, and the Last Glacial Maximum over western Europe. *Journal of Geophysical Research* 109, D08104. doi:10.1029/2003JD004161.
- Jansen, E., Overpeck, J., Briffa, K.R., Duplessy, J.-C., Joos, F., Masson-Delmotte, V., Olago, D., Otto-Bliesner, B., Peltier, W.R., Rahmstorf, S., Ramesh, R., Raynaud, D., Rind, D., Solomina, O., Villalba, R., Zhang, D., 2007. Palaeoclimate. In: Solomon, S., Qin, D., Manning, M., Chen, Z., Marquis, M., Averyt, K.B., Tignor, M., Miller, H.L. (Eds.), *Climate Change 2007: The Physical Science Basis. Contribution of Working Group I to the Fourth Assessment Report of the Intergovernmental Panel on Climate Change*. Cambridge University Press, Cambridge, United Kingdom and New York, NY, USA, pp. 434–497.
- Jiang, D., 2008. Vegetation and soil feedbacks at the Last Glacial Maximum. *Palaeogeography, Palaeoclimatology, Palaeoecology* 268, 39–46.
- Jiang, D., Lang, X., 2010. Last Glacial Maximum East Asian monsoon: results of PMIP simulations. *Journal of Climate* 23, 5030–5038.
- Jiang, D., Wang, H.J., Drange, H., Lang, X., 2003. Last Glacial Maximum over China: sensitivities of climate to paleovegetation and Tibetan ice sheet. *Journal of Geophysical Research* 108 (D3), 4102. doi:10.1029/2002JD002167.
- Joussaume, S., Taylor, K.E., 1995. Status of the Paleoclimate Modeling Intercomparison Project (PMIP). In: Gates, W.L. (Ed.), *Proceedings of the First International AMIP Scientific Conference*. World Meteorol. Org., Geneva, pp. 425–430. WCRP-92, WMO/TD-732.
- Ju, L.X., Wang, H.J., Jiang, D., 2007. Simulation of the Last Glacial Maximum climate over East Asia with a regional climate model nested in a general circulation model. *Palaeogeography, Palaeoclimatology, Palaeoecology* 248, 376–390.
- Kageyama, M., Peyron, O., Pinot, S., Tarasov, P., Guiot, J., Joussaume, S., Ramstein, G., 2001. The last glacial maximum over Europe and western Siberia: a PMIP comparison between models and data. *Climate Dynamics* 17, 23–43.
- Kageyama, M., Laine, A., Abe-Ouchi, A., Braconnot, P., Cortijo, E., Crucifix, M., de Vernal, A., Guiot, J., Hewitt, C.D., Kitoh, A., Kucera, M., Marti, O., Ohgaito, R., Otto-Bliesner, B., Peltier, W.R., Rosell-Melé, A., Vettoretti, G., Weber, S.L., Yu, Y., MARGO Project Members, 2006. Last Glacial Maximum temperatures over the North Atlantic, Europe and western Siberia: a comparison between PMIP models, MARGO sea-surface temperatures and pollen-based reconstructions. *Quaternary Science Reviews* 25, 2082–2102.
- Kalnay, E., Kanamitsu, M., Kistler, R., Collins, W., Deaven, D., Gandin, L., Iredell, M., Saha, S., White, G., Woollen, J., Zhu, Y., Chelliah, M., Ebisuzaki, W., Higgins, W., Janowiak, J., Mo, K.C., Ropelewski, C., Wang, J., Leetmaa, A., Reynolds, R., Jenne, R., Joseph, D., 1996. The NCEP/NCAR reanalysis project. *Bulletin of the American Meteorological Society* 77, 437–472.
- Levis, S., Foley, J.A., Pollard, D., 1999. CO₂, climate, and vegetation feedbacks at the Last Glacial Maximum. *Journal of Geophysical Research* 104 (D24), 31191–31198.
- Liu, K.-B., 1988. Quaternary history of the temperate forests of China. *Quaternary Science Reviews* 7, 1–20.
- Liu, X., Wu, X., Dong, G., Dong, B., Valdes, P.J., 1995. A modeling research on East Asia monsoonal climate at the Last Glacial Maximum (in Chinese). *Scientia Meteorologica Sinica* 15, 183–196.
- Liu, J., Yu, G., Chen, X., 2002. Palaeoclimate simulation of 21 ka for the Tibetan Plateau and Eastern Asia. *Climate Dynamics* 19, 575–583.
- Lu, H.-Y., Wu, N.-Q., Liu, K.-B., Jiang, H., Liu, T.-S., 2007. Phytoliths as quantitative indicators for the reconstruction of past environmental conditions in China II: palaeoenvironmental reconstruction in the Loess Plateau. *Quaternary Science Reviews* 26, 759–772.
- Masson-Delmotte, V., Kageyama, M., Braconnot, P., Charbit, S., Krinner, G., Ritz, C., Guilyardi, E., Jouzel, J., Abe-Ouchi, A., Crucifix, M., Gladstone, R.M., Hewitt, C.D., Kitoh, A., LeGrande, A.N., Marti, O., Merkel, U., Motoi, T., Ohgaito, R., Otto-Bliesner, B., Peltier, W.R., Ross, I., Valdes, P.J., Vettoretti, G., Weber, S.L., Wolf, F., Yu, Y., 2006. Past and future polar amplification of climate change: climate model intercomparisons and ice-core constraints. *Climate Dynamics* 26, 513–529.
- Monnin, E., Indermuhle, A., Dallenbach, A., Fluckiger, J., Stauffer, B., Stocker, T.F., Raynaud, D., Barnola, J.M., 2001. Atmospheric CO₂ concentrations over the last glacial termination. *Science* 291, 112–114.
- Otto-Bliesner, B.L., Schneider, R., Brady, E.C., Kucera, M., Abe-Ouchi, A., Bard, E., Braconnot, P., Crucifix, M., Hewitt, C.D., Kageyama, M., Marti, O., Paul, A., Rosell-Melé, A., Waelbroeck, C., Weber, S.L., Weintelt, M., Yu, Y., 2009. A comparison of PMIP2 model simulations and the MARGO proxy reconstruction for tropical sea surface temperatures at last glacial maximum. *Climate Dynamics* 32, 799–815.
- Peltier, W.R., 1994. Ice age paleogeography. *Science* 265, 195–201.
- Peltier, W.R., 2004. Global glacial isostasy and the surface of the ice-age earth: the ICE-5G (VM2) model and GRACE. *Annual Review of Earth and Planetary Sciences* 32, 111–149.
- Pinot, S., Ramstein, G., Harrison, S.P., Prentice, I.C., Guiot, J., Stute, M., Joussaume, S., 1999. Tropical paleoclimates at the Last Glacial Maximum: comparison of Paleoclimate Modeling Intercomparison Project (PMIP) simulations and paleodata. *Climate Dynamics* 15, 857–874.
- Ramstein, G., Kageyama, M., Guiot, J., Wu, H., Hély, C., Krinner, G., Brewer, S., 2007. How cold was Europe at the Last Glacial Maximum? A synthesis of the progress achieved since the first PMIP model-data comparison. *Climate of the Past* 3, 331–339.
- Raynaud, D., Jouzel, J., Barnola, J.M., Chappellaz, J., Delmas, R.J., Lorius, C., 1993. The ice record of greenhouse gases. *Science* 259, 926–934.
- Shi, Y., 2002. Characteristics of late Quaternary monsoonal glaciation on the Tibetan Plateau and in East Asia. *Quaternary International* 97–98, 79–91.
- Shi, Y., Zheng, B., Yao, T., 1997. Glaciers and environments during the Last Glacial Maximum (LGM) on the Tibetan Plateau (in Chinese). *Journal of Glaciology and Geocryology* 19, 97–113.
- Su, Z., Ma, Y., 1997. The discovery of palaeo-eolian formed in the last glacial maximum and environmental evolution in the Northwest of Shanxi (in Chinese). *Journal of Desert Research* 17, 389–394.
- Tang, L.Y., Shen, C.M., Kong, Z.Z., Wang, F.B., Liu, K.B., 1998. Pollen evidence of climate during the Last Glacial Maximum in eastern Tibetan Plateau (in Chinese). *Journal of Glaciology and Geocryology* 20, 133–140.
- Tang, L.Y., Shen, C.M., Liu, K.B., Yu, S.Y., Li, C.H., 2004. Climatic changes in the southeastern Qinghai-Tibetan Plateau during the Last Glacial Maximum – pollen records from southeastern Tibet (in Chinese). *Science in China (Series D)* 34, 436–442.
- Tao, S.Y., Chen, L.X., 1987. A review of recent research on the East Asian monsoon in China. In: Chang, C.-P., Krishnamurti, T.N. (Eds.), *Monsoon Meteorology*. Oxford University Press, pp. 60–92.
- Wan, H.W., Tang, L.Y., Zhang, H.C., Li, C.H., Pang, Y.Z., 2008. Pollen record reflects climate changes in eastern Qaidam Basin during 36–18 ka B.P. (in Chinese). *Quaternary Sciences* 28, 112–121.
- Wang, H.J., Zeng, Q.C., 1993. The numerical simulation of the ice age climate. *Acta Meteorologica Sinica* 7, 423–430.
- Wang, N.-A., Wang, T., Shi, Z.-T., Hu, G., Gao, S.-W., 2001. The discovery of sand wedges of the last glaciation in the Hexi Corridor and its paleoclimatic significance (in Chinese). *Journal of Glaciology and Geocryology* 23, 46–50.
- Wang, Y.J., Kong, X.G., Shao, X.H., Wu, J.Y., 2002. Century-scale climatic oscillations during the last glacial maximum recorded in a stalagmite from Nanjing (in Chinese). *Quaternary Sciences* 22, 243–251.

- Wu, N.Q., Lü, H.Y., Sun, X.J., Guo, Z.T., Liu, J.Q., Han, J.M., 1994. Climate transfer function from opal phytolith and its application in paleoclimate reconstruction of China loess-paleosol sequence (in Chinese). *Quaternary Sciences* 14, 270–279.
- Xie, P., Arkin, P.A., 1997. Global precipitation: A 17-year monthly analysis based on gauge observations, satellite estimates, and numerical model outputs. *Bulletin of the American Meteorological Society* 78, 2539–2558.
- Yao, T., Liu, X., Wang, N., Shi, Y., 2000. Amplitude of climatic changes in Qinghai–Tibetan Plateau. *Chinese Science Bulletin* 45, 1236–1243.
- Yu, G., Chen, X., Liu, J., Wang, S., 2001. Preliminary study on LGM climate simulation and the diagnosis for East Asia. *Chinese Science Bulletin* 46, 364–368.
- Yu, G., Xue, B., Liu, J., Chen, X., 2003. LGM lake records from China and an analysis of climate dynamics using a modelling approach. *Global and Planetary Change* 38, 223–256.
- Zhang, B.Z., Zhang, P.X., Lowenstein, T.K., Spencer, R.J., 1995. Time range of the great ice age of the last glacial stage and its related geological event of playa in the Qinghai–Xizang (Tibet) Plateau (in Chinese). *Quaternary Sciences* 15, 193–201.
- Zhao, P., Chen, L.X., Zhou, X.J., Gong, Y.F., Han, Y., 2003. Modeling the East Asian climate during the last glacial maximum. *Science in China (Series D)* 46, 1060–1068.
- Zheng, Z., Guiot, J., 1999. A 400000-year paleoclimate reconstruction in tropical region of China (in Chinese). *Acta Scientiarum Naturalium Universitatis Sunyatseni* 38, 94–98.
- Zheng, Y.Q., Yu, G., Wang, S.M., Xue, B., Zhuo, D.Q., Zeng, X.M., Liu, H.Q., 2004. Simulation of paleoclimate over East Asia at 6 ka BP and 21 ka BP by a regional climate model. *Climate Dynamics* 23, 513–529.